

Cluster modeling and coordination structures of Cu⁺ ions in Al-incorporated Cu-MEL catalysts – a density functional theory study

Mehdi Ghambarian,¹ Zahra Azizi,² and Mohammad Ghashghaee,^{3*}

¹ Gas Conversion Department, Faculty of Petrochemicals, Iran Polymer and Petrochemical Institute, P.O. Box 14975-112, Tehran, Iran.

² Department of Chemistry, Karaj Branch, Islamic Azad University, P.O. Box 31485-313, Karaj, Iran

³ Faculty of Petrochemicals, Iran Polymer and Petrochemical Institute, P.O. Box 14975-112, Tehran, Iran

* Corresponding author. Tel.: +98 21 48662481; fax: +98 21 44787032. *E-mail address:* m.ghashghaee@ippi.ac.ir

Abbreviated running title: *DFT modeling of Cu-ZSM-11 catalysts*

Received July 8th, 2016; Accepted December 2nd, 2016.

Abstract. A density-functional-based cluster modeling was implemented on the Al-incorporated Cu-MEL zeolite catalyst (Cu-ZSM-11) to probe the electronic, energetic and structural features of the active sites of the catalyst at the B3LYP/6-311+G* and M06/Def2-TZVP levels. The HOMO–LUMO energy gap fell into the range of 3.31–5.15 eV at TD-BH&HLYP/6-311+G* with the lowest magnitude for the I–Cu and M1–Cu clusters. Population-averaged values for the exchange enthalpy and binding energy were also calculated, being approximately 125 and 171 kcal/mol, respectively.

Keywords: Copper; MEL zeolite; DFT modeling; ZSM-11 catalysts; QTAIM.

Resumen: El modelado de clústers empleando métodos derivados de la teoría de funcionales de la densidad fue aplicado al catalizador Cu-MEL ceolita que incorpora aluminio (Cu-ZSM-11) para probar las características electrónicas, energéticas y estructurales del sitio activo del catalizador con los niveles de teoría B3LYP/6-311+G* y M06/Def2-TZVP. La separación energética entre los orbitales HOMO y LUMO se encontró en el rango de 3.31 a 5.15 eV a nivel BH&HLYP/6-311+G, teniendo el menor valor para los clústers I-Cu y M1-Cu. También se determinaron los valores promedio de la población para la entalpía de intercambio y la energía de unión, con valores de 125 y 171 kcal/mol respectivamente.

Palabras clave: cobre; MEL ceolita; modelado empleando DFT; catalizador ZSM-11; QTAIM.

Introduction

Transition-metal ions (TMIs) incorporated into zeolitic frameworks are known as active heterogeneous catalysts for numerous applications [1-3]. There has been fairly extensive research into copper ions impregnated over different supports [1, 4-17], which serve as efficient catalysts for a wide range of reactions, such as, methanol synthesis, oxidation of hydrocarbons, carbonylation of methanol, pollutant abatement, and hydrogenation reactions [4-6, 18]. Among different metal exchanged zeolites, e.g., Cu-ZSM-5 proved to be the most active catalyst for direct decomposition of NO [8].

There exist several reports on the experimental identification as well as theoretical modeling of copper ions in porous materials [2, 4, 6-7, 17-38]. Meanwhile, the monovalent copper ion has received substantial interest. The adsorption of various probe molecules such as NO_x, CO_x, N₂, O₂, and H₂O on the Cu⁺ ions exchanged into an MFI zeolite has been the subject of several studies [1, 7-9, 13-14, 20, 22, 37, 39-51]. The quantum chemical calculations have shown in accordance with IR measurements that the NO molecule is more freely activated on Cu⁺ centers than on Cu²⁺ as evinced by the remarkably higher HOMO level of the former [20]. Unusual σ -type adsorption complexes with both hydrogen molecule and

light alkanes have been indicated for the Cu⁺ ion, compared to other cations (e.g., Li⁺ or Mg²⁺) [17]. The Cu⁺-exchanged zeolites are very promising adsorbents for the separation of olefins and desulfurization of fossil fuels [18].

Zeolite ZSM-11 is the most symmetrical pentasil observed so far [52]. The framework of ZSM-11 (MEL type) involves pentasil layers joined enantiomerically through σ -reflection, forming a two-dimensional network of straight channels with perpendicular intersections [52-54]. Experimental studies have demonstrated that both Cu-ZSM-11 (with MEL structure type with two-dimensional 10T-ring pores) and Cu-ZSM-12 (MTW structure of one-dimensional 12T-ring pores) are about twice as active as the most investigated zeolite Cu-ZSM-5 (MFI structure with straight and zig-zag/sinusoidal channels) in direct decomposition of NO [11, 27]. It was suggested that there must be a preferential formation of active sites and/or better accessibility in the straight channels compared to the sinusoidal ones, which explains the higher activity of ZSM-11 material [11]. Analogously, the Cu-ZSM-11 catalyst has been applied to direct N₂O decomposition where it was obviously more active than Cu-ZSM-5 with the same Si/Al ratio [55]. Synthesized mesoporous H-ZSM-11 catalysts have also shown extraordinary high activities in conversion of *n*-hexadecane [56].

It is believed that the coordination of the cation by the zeolite framework is vital for the catalytic properties of copper ions as the counterpart gas-phase ions do not confer such an activity [18]. DFT calculations have shown, e.g., that the interactions of NO with the gas-phase isolated Cu^+ ions are essentially different from those inside a zeolite structure. The former system showed interactions of the a' singly occupied orbital (SOMO) of NO with the unoccupied 4s and the occupied 3d orbitals of Cu^+ which depopulated the antibonding SOMO thus reinforcing the NO bond. In contrast, the Cu-zeolite system showed increased Pauli repulsions due to electrostatic attractions which led to higher level (occupied) 3d orbitals interacting with the a'' LUMO of NO molecule; these interactions populated the antibonding LUMO of NO and, hence, weakened the NO bond [7].

Despite the relative importance of the MEL-type materials, really scant attention has been directed in theoretical studies toward these catalysts [57-59]. The purpose of this paper is then to investigate the coordination, local structure and properties of Cu^+ ions at different positions within a ZSM-11 lattice. Knowledge of the properties of these cationic sites would be essential for a better understanding of their catalytic behaviors which facilitates their improvement and replacement with new zeolite-based catalysts.

Results and discussion

The overview of possible exchange sites in the porous network of an MEL-type zeolite is shown in Fig. 1, which illustrates an intersection site I, ring sites of M1, M2, M3, and M4 located in

the main channels with an increasing number of T atoms from left to right, and cage-like positions C1 and C2 that resemble a curved 6T-ring site inside the walls of ZSM-11 composed of several fused 5T-rings.

As also mentioned above, the quantum-chemical studies of the deposition and binding of small metal particles on oxide surfaces are very important for obtaining an accurate description of the catalyst interface [4]. A major challenge concerning the structural characterization of metal-ion-exchanged zeolites, in general, is to find out where the cation substitution takes place and how metal ions are coordinated to the substituted sites [28]. As can be seen in Table 1 and Fig. 1, total of 7 sites were considered for Cu^+ exchange in ZSM-11, together with a representative A site from an MFI structure for comparison. The exchange sites of C1 and C2 have the same local environment in the solid matrix, but with Al incorporation at the T6 and T1 positions, respectively. The C sites in ZSM-11 are the most similar to the A site in ZSM-5, except that the C sites are not as readily accessible to guest molecules as the A site is. This subtle difference and similar differences in the accessibility and local configurations can evidently cause discrepancies in the bulk catalytic behavior of the two pentasil solids, even if the shape and population of exchange sites were identical in both cases. The other sites of the ZSM-11 catalyst are accessible to the coming molecules almost identically, provided that the pore diffusion effects in the similar cavities are the same.

At the first sight, one may think that few Al atoms have been considered here with respect to the framework Si atoms. Therefore, in reality, there must be some other Al atoms as well that influence the local environment of the Cu ions and

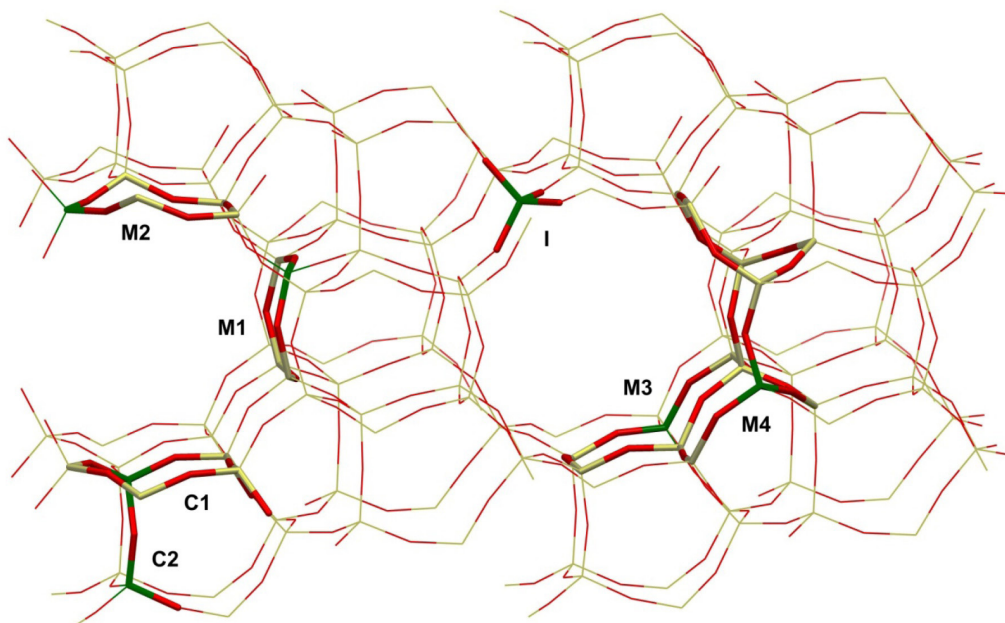


Fig. 1. Different positions for the placement of the Cu^+ ions in the ZSM-11 zeolite framework viewed at the (010) layer. The 10T-rings represent the main channels of the zeolite lattice.

the considered intra-framework Al ones. However, we considered only one Al ion at each site. This is an assumption that is made not only for the simplicity of the calculations, but rather from a realistic point of view. In theory, the number of Al atoms in a zeolitic material is only limited by the Loewenstein rule (no adjacent Al tetrahedra) which requires Si/Al ratios larger than 1. However, the MEL and MFI structures are normally listed as high-silica materials with a lower practical limit of 10 or 11 for the Si/Al ratio [60-64]. Moreover, most of catalytic applications require moderate Si/Al ratios to ascertain a balance between the number of acidic sites and the acid strength and hence for an optimum performance [60, 62, 65-66]. The local Si/Al ratios obtained from the atomic population in the isolated clusters lie in the range of 3–8, which are quite smaller than the observed lower limit above for an entire unit cell. Also worth noting is that the simulated acidic sites have a number of shared silicon atoms, making the average Si/Al ratio further smaller. The possibilities for Al substitution and the subsequent models simulated here are then realistic and comprehensive enough, assuming a uniform substitution of the Al atoms. Zeolite samples with higher Si/Al ratios can be modeled systematically by reducing the Al substitution sites according to their thermodynamic favorability. The same discussion holds for the Cu atoms assuming a one-by-one stoichiometric substitution of the exchangeable protons with the Cu⁺ ions. In addition, our preliminary studies [67-68] indicated the suitability of the cut-out clusters in modeling of the Cu-ZSM-11 catalyst in terms of thermodynamics, geometrical features, and HOMO–LUMO

gaps and in addressing the border and confinement effects [69-74] normally contributing in microporous materials.

The optimized geometries of the Cu⁺ active sites are shown in Fig. 2 for which Table 1 presents the highest occupied molecular orbital (HOMO) and the lowest unoccupied molecular orbital (LUMO) energy levels and their corresponding HOMO–LUMO gaps. The coordination states of copper in the cluster models shown in Fig. 2 have been determined from the electronic data reported in Table 3 (vide infra). Overall, the coordination of the copper ion is twofold in I–Cu, M1–Cu, and M4–Cu, threefold in C1–Cu, and fourfold in M2–Cu, M3–Cu, C2–Cu, and A–Cu. As it is seen, the incorporation of Al atom at the T1 position in the cage-like C2 site provides a higher coordination number for the Cu⁺ ion than that encompassing the Al atom at the T6 position (C1). Moreover, the corresponding site from ZSM-11 (C2) that resembles the alpha-site of ZSM-5 (A) has the same coordination number of four.

Table 1 may be used to draw some information about the available sites of the Cu-ZSM-11 in terms of reactivity. It has to be mentioned, however, that the exchange reactions and the catalysis events over the formed active sites are all of a transient nature where the reactants interact and their properties change continually upon approaching the active site. These aspects are normally studied using molecular dynamics simulations at the first-principles level [75-79]. For the comparisons made herein, it will be assumed that the distribution of the Cu⁺ ions at the exchange locations and the following

Table 1. Calculated HOMO and LUMO energy levels and HOMO–LUMO energy gaps (eV) at B3LYP/6-311+G*, M06/Def2-TZVP, TD-B3LYP/6-311+G*, and TD-BH&HLYP/6-311+G* for the Cu⁺ active sites where the LUMO eigenvalue for the two latter was calculated by subtracting the HOMO eigenvalue from the HOMO–LUMO gap.

| Cluster | E_{HOMO} | E_{LUMO} | $\Delta E_{\text{HOMO-LUMO}}$ | E_{HOMO} | E_{LUMO} | $\Delta E_{\text{HOMO-LUMO}}$ |
|---------|-------------------|-------------------|-------------------------------|---------------------|-------------------|-------------------------------|
| | B3LYP/6-311+G* | | | M06/Def2-TZVP | | |
| I–Cu | –6.77 | –2.72 | 4.05 | –7.41 | –2.67 | 4.74 |
| M1–Cu | –6.95 | –3.11 | 3.84 | –7.23 | –3.02 | 4.21 |
| M2–Cu | –6.50 | –2.17 | 4.33 | –7.06 | –2.11 | 4.95 |
| M3–Cu | –5.45 | –1.12 | 4.33 | –6.08 | –0.87 | 5.21 |
| M4–Cu | –6.92 | –1.91 | 5.00 | –7.20 | –1.84 | 5.36 |
| C1–Cu | –6.53 | –1.62 | 4.90 | –6.95 | –1.35 | 5.60 |
| C2–Cu | –6.72 | –1.93 | 4.78 | –6.97 | –1.75 | 5.21 |
| A–Cu | –6.31 | –1.55 | 4.75 | –6.90 | –1.52 | 5.38 |
| | TD-B3LYP/6-311+G* | | | TD-BH&HLYP/6-311+G* | | |
| I–Cu | –6.77 | –4.30 | 2.47 | –8.77 | –5.46 | 3.31 |
| M1–Cu | –6.95 | –3.92 | 3.03 | –8.70 | –4.76 | 3.95 |
| M2–Cu | –6.50 | –3.72 | 2.78 | –8.66 | –4.95 | 3.71 |
| M3–Cu | –5.45 | –2.31 | 3.14 | –7.71 | –3.56 | 4.16 |
| M4–Cu | –6.92 | –2.56 | 4.35 | –8.51 | –3.36 | 5.15 |
| C1–Cu | –6.53 | –2.55 | 3.98 | –8.55 | –3.64 | 4.91 |
| C2–Cu | –6.72 | –2.90 | 3.82 | –8.54 | –3.75 | 4.79 |
| A–Cu | –6.31 | –3.09 | 3.22 | –8.54 | –4.37 | 4.17 |

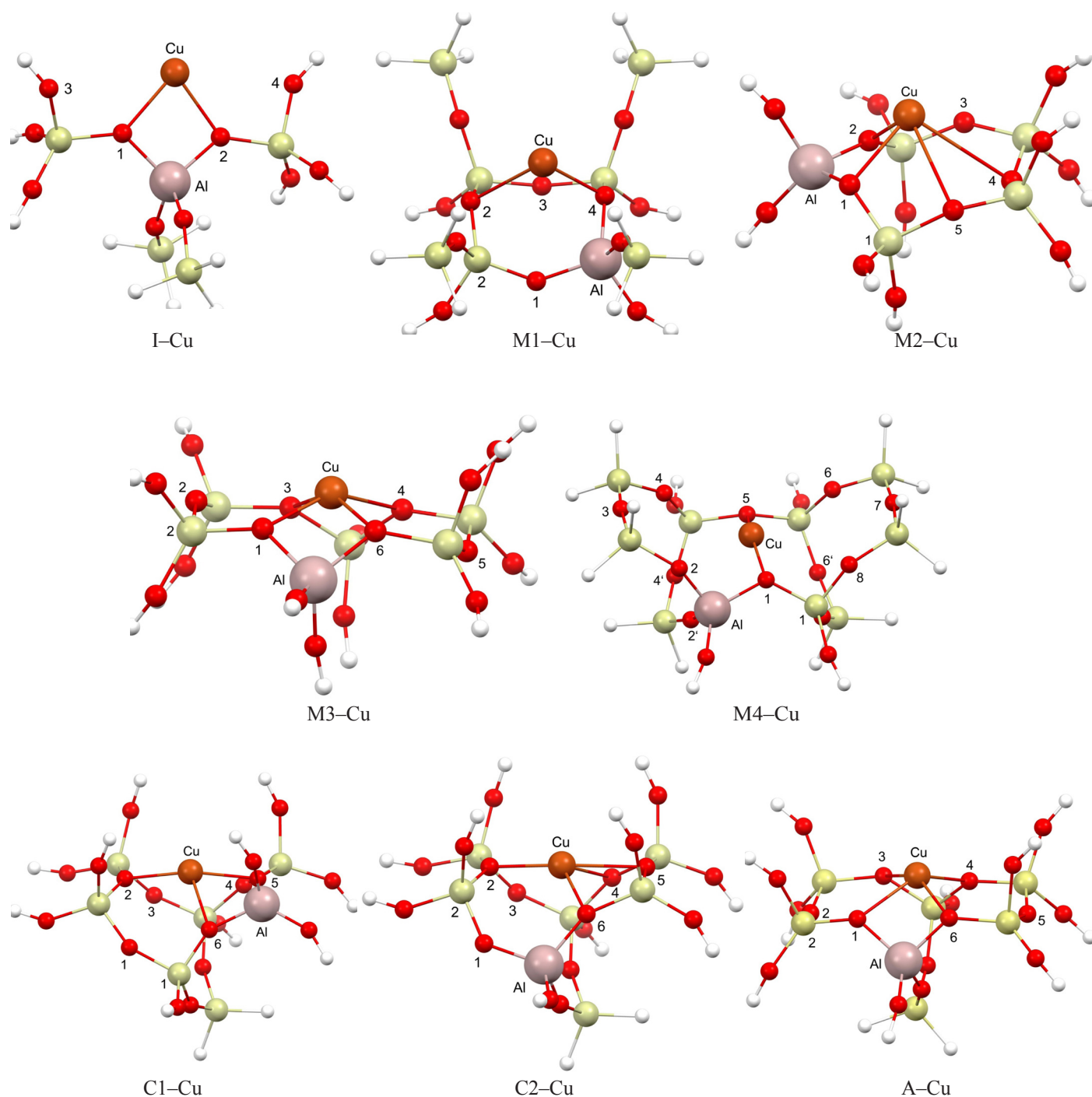


Fig. 2. Optimized geometries of the main Cu-MEL models. The darker (in red) atoms refer to lattice oxygen, the plain bigger balls of the framework (in yellow) represent silicon atoms, the copper ions are shown in brown, the aluminum substitutions are marked in violet, and the terminal white balls indicate saturating hydrogen atoms (For the color version of this figure, please refer to the electronic version of this article). The copper and aluminum atoms have also been labeled on each site for clarity.

reactivity-related consequences are determined by their thermodynamic favorability rather than by any kinetic events as also adopted earlier [57, 80-82]. Supplementary comments will be made on the accessibility of the active sites for the reactant molecules, however. Although hybrid functionals (such as

B3LYP and M06) generally predict accurate HOMO-LUMO gaps in transition-metal exchanged zeolites [83-84], Zhang and Musgrave [85] reported after careful analysis against experimental lowest excitation energies of a number of molecules that only time-dependent (TD) DFT methods accurately predict

the HOMO–LUMO gaps. Therefore, we included also the TD-B3LYP and TD-BH&HLYP [86–87] functionals in evaluating the frontier orbital energy data. Moreover, the discussion made here on the reactivity-driven electron transfer tendency of the CuZ sites with respect to an adsorbate should not be confused with the standard definitions of electrodonating and electroaccepting powers [88–91].

Wherever the Cu-MEL catalyst can play the role of an electron donor with respect to an adsorbate species, a higher HOMO energy level of the CuZ means a higher propensity for electron donation to the LUMO of the guest molecule. Here, the M3–Cu structure (with the HOMO levels of –6.08 eV at M06/Def2-TZVP and –7.71 at TD-BH&HLYP/6-311+G*) presents the highest reactivity towards a stronger electron-acceptor species/ligand. In contrast, the I–Cu and M1–Cu sites were presented by different methods to be the least reactive sites in terms of the HOMO level; the coordination number of copper in both of them is two while in M3–Cu is four (Fig. 2), however. The findings are then generally consistent with the trends reported in the literature [48–49] stating that the electron-donation power of the active site correlates well with the degree of coordination. The HOMO energy level of A–Cu differed from –8.54 eV to –6.31 eV which was slightly lower than the previously reported magnitude of –5.17 eV by Broclawik et al. [20] for Cu⁺ exchanged into an alpha-site of ZSM-5. Apart from a difference in the level of the computations or the computational methods, the differences may be attributed to the fact that two Al atoms were present at the T1 and T4 positions in that paper.

When CuZ clusters can accept electrons from a stronger donor, such as ammonia [19], a lower LUMO energy level translates into an easier reaction with the guest molecule. As apparent from Table 1, a reverse trend compared to what explained for the HOMO level is true for the LUMO level, i.e., the I–Cu and M1–Cu sites are predicted to be the best electron acceptors from the HOMO of a guest molecule within the framework of the frontier molecular orbital (FMO) theory [92]. On the contrary, the LUMO level of the M3–Cu site stands higher than any other site according to most of the methods, indicating its weakest electron-accepting property. Comparing the HOMO and LUMO levels of the A–Cu site with those of its equivalent in MEL structure (C2–Cu), one may conclude that the resemblance of the geometries from two similar pentasil materials in terms of the ring size will not assure similarities between all of their properties. The same issue holds true for the two cage-like structures with Al replacement at T1 or T6 positions.

As it is well-known [93–97], a relatively small gap between the HOMO and LUMO energy levels reflects a high polarizability, less significant hardness, and higher reactivity. Whereas most of the methods predicted M4–Cu as the most stable site, the I–Cu and M1–Cu clusters were estimated as the most reactive. Despite the general trends observed, no significant correlation could be established between the HOMO–LUMO gaps by methods of different category. We note, however, that some linear correlations exist between the

frontier orbital energy levels predicted by the two methods within each category (see Supporting Information, Fig. S1).

The bond critical point properties determined for the CuZ clusters are shown in Table 2 which indicates low electron densities with a local depletion of the internuclear densities for all of the investigated sites. This agrees with the general expectation that metal–oxygen interactions are normally characterized through positive values of $\nabla^2\rho$ at the BCP [13]. According to the quantum theory of atoms in molecules (QTAIM) [98–99], the existence of a (3, –1) critical point in the electron density distribution along the path between a pair of atoms indicates that the electron density is localized in the binding region between the nuclei, thus being an indicator of the presence of a chemical bond. Moreover, the electron density at BCP may be regarded as a direct indicator of the bond order. Based on the QTAIM calculations, the nature of the chemical bonds may be described in terms of electron density $\rho(r)$ and the corresponding Laplacian $\nabla^2\rho(r)$ at the bond critical point (BCP). According to this theory, $\nabla^2\rho(r)$ provides information about the electronic charge and the degree of local depletion or concentration of the interatomic densities [13, 99]. The positive values of $\nabla^2\rho(r)$ point to closed-shell electrostatic interactions, particularly because the $|\lambda_1|/\lambda_3$ ratio is much smaller than 1. However, the intrinsic nature of the electron density distributions in the interatomic region of the interactions entail that the positive eigenvalue of the Hessian matrix at the BCP decreases with increasing the Cu–O bond distances, thus rendering systematic reductions in $\nabla^2\rho(r)$ (vide infra). The QTAIM calculations led to no BCP data for the copper–silicon or copper–aluminum interactions.

Table 3 reports the NBO charges of Cu, Al, and O atoms in the CuZ clusters where a partial charge transfer from the zeolite substrate to the orbitals of the metal is clear. Earlier studies have also shown that the positive charge of the Cu ion shrinks upon adsorption on a zeolite surface owing to remarkable charge transfers from the siloxy groups of the surface to the metal ion [33, 100–101]. An opening (hybridization) of the *d*-shell on the Cu⁺ is a requisite for this electron transfer [7]. The most positive charge on Cu⁺ is observed for the I–Cu cluster (0.898 e) while the highest deviation from the formal cationic charge of +1 is found on C1–Cu and C2–Cu with interestingly similar charges (0.672 e). As a result, the highest charge transfer from the surface to the cation occurs at the cage-like positions as comprehended from a shrinkage of the positive charge of Cu cation with respect to its formal charge. This charge transfer varied from 0.10 e to 0.33 e; these values were in agreement with the lower limit (0.33 e) reported for the Cu_nO clusters [102] and very similar to the values obtained for other complexes of Cu(I) [103–104]. At the same time, no one-to-one relationship could be established between the amount of charge transfer and coordination number of Cu ion.

Table 4 contains the bond lengths for all of the Cu-ZSM-11 cluster models. The three smallest Cu–O bond lengths (1.925, 1.939, and 1.946 Å) belong to the M4–Cu, C1–Cu, and C2–Cu sites, respectively. The minimum $r(\text{Cu–Al})$

Table 2. Topological properties of the Cu–O bonds at the bond critical point for the investigated Cu/ZSM-11 catalysts at the B3LYP/6-311+G* level.

| Cluster | Cu–O1 | | | | | Cu–O2 | | | | |
|---------|--------|-------------|-------------|-------------|----------------|--------|-------------|-------------|-------------|----------------|
| | ρ | λ_1 | λ_2 | λ_3 | $\nabla^2\rho$ | ρ | λ_1 | λ_2 | λ_3 | $\nabla^2\rho$ |
| I–Cu | 0.069 | –0.084 | –0.083 | 0.528 | 0.362 | 0.072 | –0.089 | –0.088 | 0.561 | 0.384 |
| M1–Cu | — | — | — | — | — | 0.043 | –0.043 | –0.040 | 0.242 | 0.159 |
| M2–Cu | 0.055 | –0.061 | –0.056 | 0.361 | 0.245 | 0.065 | –0.077 | –0.074 | 0.477 | 0.326 |
| M3–Cu | 0.062 | –0.074 | –0.070 | 0.450 | 0.306 | — | — | — | — | — |
| M4–Cu | 0.090 | –0.125 | –0.123 | 0.772 | 0.523 | — | — | — | — | — |
| C1–Cu | — | — | — | — | — | 0.080 | –0.104 | –0.104 | 0.681 | 0.473 |
| C2–Cu | — | — | — | — | — | 0.085 | –0.115 | –0.114 | 0.735 | 0.505 |
| A–Cu | 0.049 | –0.052 | –0.047 | 0.306 | 0.207 | — | — | — | — | — |
| | Cu–O3 | | | | | Cu–O4 | | | | |
| | ρ | λ_1 | λ_2 | λ_3 | $\nabla^2\rho$ | ρ | λ_1 | λ_2 | λ_3 | $\nabla^2\rho$ |
| I–Cu | — | — | — | — | — | — | — | — | — | — |
| M1–Cu | — | — | — | — | — | 0.077 | –0.098 | –0.095 | 0.600 | 0.408 |
| M2–Cu | — | — | — | — | — | 0.014 | –0.011 | –0.008 | 0.064 | 0.045 |
| M3–Cu | 0.034 | –0.035 | –0.032 | 0.196 | 0.129 | 0.029 | –0.028 | –0.025 | 0.155 | 0.102 |
| M4–Cu | — | — | — | — | — | — | — | — | — | — |
| C1–Cu | — | — | — | — | — | — | — | — | — | — |
| C2–Cu | — | — | — | — | — | 0.019 | –0.015 | –0.007 | 0.084 | 0.062 |
| A–Cu | 0.013 | –0.010 | –0.005 | 0.059 | 0.044 | 0.032 | –0.032 | –0.030 | 0.178 | 0.116 |
| | Cu–O5 | | | | | Cu–O6 | | | | |
| | ρ | λ_1 | λ_2 | λ_3 | $\nabla^2\rho$ | ρ | λ_1 | λ_2 | λ_3 | $\nabla^2\rho$ |
| I–Cu | — | — | — | — | — | — | — | — | — | — |
| M1–Cu | — | — | — | — | — | — | — | — | — | — |
| M2–Cu | 0.019 | –0.016 | –0.008 | 0.088 | 0.064 | — | — | — | — | — |
| M3–Cu | — | — | — | — | — | 0.059 | –0.067 | –0.064 | 0.410 | 0.279 |
| M4–Cu | 0.068 | –0.083 | –0.083 | 0.544 | 0.377 | — | — | — | — | — |
| C1–Cu | 0.088 | –0.118 | –0.118 | 0.743 | 0.506 | 0.046 | –0.046 | –0.042 | 0.269 | 0.181 |
| C2–Cu | 0.050 | –0.052 | –0.047 | 0.316 | 0.217 | 0.072 | –0.086 | –0.084 | 0.539 | 0.369 |
| A–Cu | — | — | — | — | — | 0.060 | –0.069 | –0.064 | 0.418 | 0.285 |

was observed for the M2–Cu site. However, the $r(\text{Cu–Al})$ in C2–Cu was the maximum $r(\text{Cu–Al})$ observed and the other $r(\text{Cu–O})$ values in C2–Cu were large. The results of Table 4 can also show that no perfect symmetrical configurations (with identical Cu–O bond lengths) as observed in the case of Zn cation interactions with an all-silica MEL structure [57] are found here for the CuZ clusters because of the presence of an Al atom in the ring sites. Table 4 also signifies a correspondence between the values of $r(\text{Cu–O})$ and $r(\text{Cu–Si})$, which is anticipated.

As expressed by Šponer *et al.* [38], the coordination of metal cations such as Cu^+ in zeolites involves an electronic perturbation of the charge distribution over the binding sites where the extent of charge transfer should correlate with the formal charge of the ion and the bond length parameters. Such a

correlation was reported previously for the interactions of Zn^{2+} adsorbed on a silicalite-2 structure [57]. Comparing the data reported in Tables 3 and 4 along with an account of the coordination numbers in Fig. 2, however, no well-developed correlations could be obtained here between the bond length parameters and the NBO charge data including $q(\text{Cu–O})$. Instead, some excellent correlations are displayed between some of the bond critical point properties and the corresponding bond lengths (Fig. 3). All of the Cu–O bonds recognized by the QTAIM approach were used to assert these correlations. The exchange and binding energies and the reported HOMO, LUMO, and HOMO–LUMO gap were independent of the bond length or the bond critical point data. The third (positive) eigenvalue of the Hessian matrix of the electron distribution at the BCP describes the local depletion of the electron density in the binding

Table 3. Partial charge of the Cu ion, Al atom and lattice O atoms in the investigated cluster models of Cu/ZSM-11 at the B3LYP/6-311+G* level.

| Cluster | Cu | Al | O1 | O2 | O3 | O4 | O5 | O6 | O7 | O8 | O2' | O4' | O6' | O8' |
|---------|-------|-------|--------|--------|--------|--------|--------|--------|--------|--------|--------|--------|--------|--------|
| I-Cu | 0.898 | 2.109 | -1.367 | -1.376 | -1.135 | -1.139 | — | — | — | — | — | — | — | — |
| M1-Cu | 0.835 | 2.047 | -1.272 | -1.275 | -1.243 | -1.351 | — | — | — | — | — | — | — | — |
| M2-Cu | 0.816 | 2.017 | -1.320 | -1.380 | -1.267 | -1.276 | -1.269 | — | — | — | — | — | — | — |
| M3-Cu | 0.781 | 2.069 | -1.359 | -1.273 | -1.279 | -1.269 | -1.269 | -1.347 | — | — | — | — | — | — |
| M4-Cu | 0.731 | 2.077 | -1.328 | -1.322 | -1.281 | -1.275 | -1.294 | -1.272 | -1.280 | -1.260 | -1.332 | -1.267 | -1.262 | -1.283 |
| C1-Cu | 0.672 | 2.055 | -1.270 | -1.307 | -1.246 | -1.282 | -1.360 | -1.347 | — | — | — | — | — | — |
| C2-Cu | 0.672 | 2.078 | -1.269 | -1.316 | -1.248 | -1.269 | -1.299 | -1.367 | — | — | — | — | — | — |
| A-Cu | 0.792 | 2.069 | -1.341 | -1.287 | -1.265 | -1.279 | -1.281 | -1.345 | — | — | — | — | — | — |

Table 4. Copper–framework atom bond lengths obtained for the optimized Cu/ZSM-11 cluster models (Å) at the B3LYP/6-31+G* level.

| Cluster | I-Cu | M1-Cu | M2-Cu | M3-Cu | M4-Cu | C1-Cu | C2-Cu | A-Cu |
|---------|-------|-------|-------|-------|-------|-------|-------|-------|
| Cu-O1 | 2.038 | 2.956 | 2.161 | 2.091 | 1.925 | 2.975 | 3.167 | 2.207 |
| Cu-O2 | 2.022 | 2.289 | 2.072 | 3.007 | 3.150 | 1.970 | 1.946 | 3.341 |
| Cu-O3 | 3.450 | 3.163 | 3.007 | 2.365 | 3.880 | 3.264 | 3.214 | 2.888 |
| Cu-O4 | 3.191 | 2.002 | 2.877 | 2.457 | 2.973 | 2.889 | 2.744 | 2.398 |
| Cu-O5 | — | — | 2.704 | 3.202 | 2.036 | 1.939 | 2.200 | 3.168 |
| Cu-O6 | — | — | — | 2.117 | 3.152 | 2.256 | 2.039 | 2.113 |
| Cu-O7 | — | — | — | — | 4.102 | — | — | — |
| Cu-O8 | — | — | — | — | 3.321 | — | — | — |
| Cu-O2' | — | — | — | — | 2.932 | — | — | — |
| Cu-O4' | — | — | — | — | 3.289 | — | — | — |
| Cu-O6' | — | — | — | — | 3.427 | — | — | — |
| Cu-O8' | — | — | — | — | 3.074 | — | — | — |
| Cu-Al | 2.743 | 2.783 | 2.617 | 2.764 | 2.837 | 2.696 | 3.058 | 2.653 |
| Cu-Si1 | 3.396 | — | 3.049 | — | 2.959 | 3.201 | — | — |
| Cu-Si2 | 3.354 | 2.889 | — | 3.247 | — | 2.856 | 2.832 | 3.368 |
| Cu-Si3 | — | 3.090 | 3.276 | 3.338 | 4.143 | 3.005 | 3.005 | 3.632 |
| Cu-Si4 | — | 3.011 | 3.415 | 2.999 | 4.052 | 3.376 | 3.293 | 3.194 |
| Cu-Si5 | — | — | 3.138 | 3.342 | 2.933 | 2.937 | 2.926 | 3.246 |
| Cu-Si6 | — | — | — | 3.253 | 3.051 | — | 2.680 | 3.180 |
| Cu-Si7 | — | — | — | — | 4.258 | — | — | — |
| Cu-Si8 | — | — | — | — | 4.347 | — | — | — |

region. As evident, this eigenvalue which is a measure of the curvatures parallel to the bond path has a descending power-law relationship with the corresponding Cu–O bond length. This inverse interconnection reflects [105] an increase in the force constant of the bond that makes the shorter Cu–O bonds more resistant to the changes due to compactions. Both of the electron density and its Laplacian show similar power-type correlations with the Cu–O bond length in the metal–zeolite system at hand, indicating that the electronic features of the Cu–O bonds in this system can be adequately determined from the bond distances (Fig. 3). The calculated bond lengths evidently correlate with $|\lambda_{1,2}|$ as well, which is not shown here for the sake of

brevity. Similar trends have been reported for the Si–O bonds in silica polymorph materials [105–106], hydrogen bonds in cyclic dimers [107], O–H interactions between interactions between *N*-butylpyridinium nitrate and thiophenic compounds [108], and Ni–Ni and Ni–S bonds [109].

Table 5 lists some important bond angles for the investigated sites. As evident from this table, the O–Cu–O bond angles vary from the largest to the smallest in the following order: C2–Cu, C1–Cu, M4–Cu, M3–Cu, M2–Cu, M1–Cu, and I–Cu. As also evidenced from the O–O–Cu bond angles in C2–Cu through M2–Cu, the Cu⁺ ion prefers an arrangement as more flattened as possible in the available ring sites.

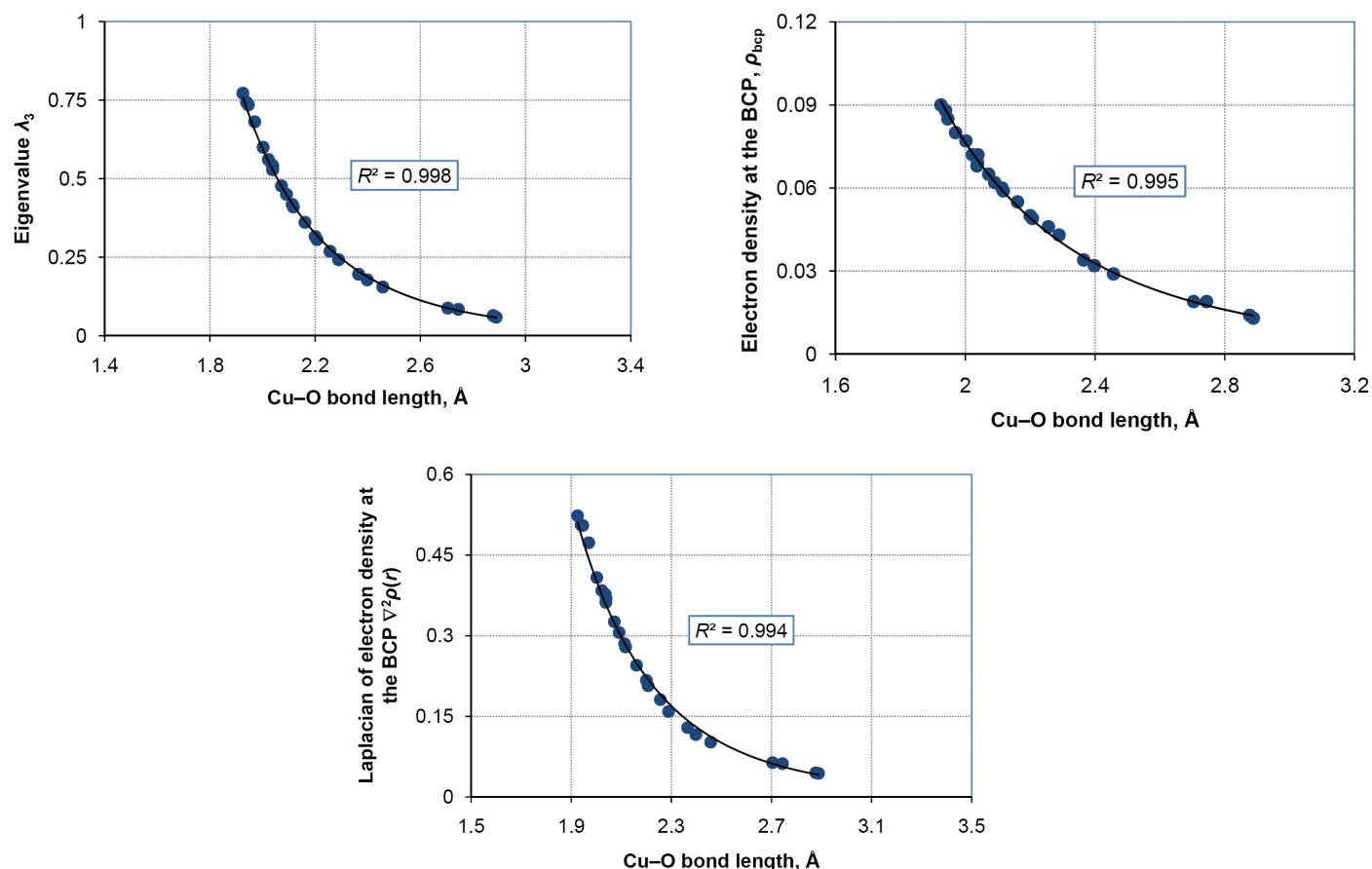


Fig. 3. Significant correlations observed between the electronic features and structural properties of the molecular models of the Cu-MEL zeolite catalyst. The fitting curves obeyed power-law functions with the exponents of -6.3 , -6.2 , and -4.6 for the correlations of λ_3 , ρ_{bcp} , and $\nabla^2\rho_{\text{bcp}}$, respectively.

No exact connection could be established between the arrangement of the Cu ion and the degree of coordination or the reactivity of the CuZ cluster in terms of the HOMO-LUMO gaps.

Table 6 reports the enthalpy and Gibbs free energy change for the exchange reaction, Eq. (2), and the energy for the metal ion binding as in Eq. (1). As evident, the enthalpy of Cu grafting for the investigated clusters ranged from 108.93 kcal/mol (M3-Cu) to 141.14 kcal/mol (M1-Cu). This indicates that the ion exchange on all of the acidic sites of ZSM-11 would be endothermic. Overall, the sequence of the thermodynamic privilege for the ion exchange is $M3 > C1 > I > A > C2 > M2 > M4 > M1$ as found from the Gibbs free energies of the exchange reaction. The most thermodynamically favored cluster to be formed is therefore the M3-Cu site followed by C1-Cu and I-Cu which cover coordination numbers of 2–4. This means that the thermodynamic favorability of the exchange reaction is not determined by the final coordination of the cation. Moreover, the data show that the ion exchange reaction is non-spontaneous at 298 K and 1 atm. Comparing the alpha site with C2 as its counterpart from ZSM-11 in terms of geometry, one can interestingly notice their close favorability for a copper/proton

Table 5. Selected bond angles for the Cu/ZSM-11 clusters (in degrees) at the B3LYP/6-31+G* level.

| Cluster | Angle (°) | Angle (°) | Angle (°) | |
|---------|-----------|-----------|-----------|-------|
| I-Cu | O1-Cu-O2 | 77.97 | — | — |
| M1-Cu | O2-Cu-O4 | 100.48 | — | — |
| M2-Cu | O2-Cu-O5 | 110.88 | O2-O4-Cu | 55.82 |
| M3-Cu | O1-Cu-O4 | 147.53 | O1-O2-Cu | 43.61 |
| M4-Cu | O1-Cu-O5 | 153.05 | O1-O2-Cu | 37.61 |
| C1-Cu | O2-Cu-O5 | 158.26 | O1-O4-Cu | 29.78 |
| C2-Cu | O2-Cu-O5 | 166.10 | O1-O4-Cu | 29.11 |
| A-Cu | O3-Cu-O6 | 145.06 | O3-O6-Cu | 20.26 |

exchange (Table 6). The results presented here also show that the cage-like locations with the Al atom at the T1 position are less prepared for a copper exchange than those with Al atom at the T6 position. As far as the most accessible sites for a coming molecule are concerned, however, both I and M3 positions are readily exchanged.

Table 6. The exchange and binding energies of the Cu⁺ ions in the active sites of ZSM-11 at the B3LYP/6-311+G* level [Please see reactions (1) and (2) in the text, respectively, for the calculation of the binding and exchange energies].

| Cluster | Population (%) | ΔE_b (kcal/mol) | ΔH_{ex} (kcal/mol) | ΔG_{ex} (kcal/mol) |
|----------------------|------------------|-------------------------|----------------------------|----------------------------|
| I-Cu | 48.1 | 174.01 | 121.11 | 128.73 |
| M1-Cu | 11.1 | 146.99 | 141.14 | 149.01 |
| M2-Cu | 14.8 | 173.04 | 129.29 | 138.73 |
| M3-Cu | 7.4 | 195.45 | 108.93 | 114.47 |
| M4-Cu | 7.4 | 161.24 | 132.41 | 144.08 |
| C1-Cu | 5.6 ^a | 174.99 | 120.47 | 127.11 |
| C2-Cu | 5.6 ^a | 158.08 | 128.11 | 137.82 |
| Overall ^b | 100 | 170.68 | 124.84 | 132.96 |
| A-Cu | — | 179.71 | 126.17 | 133.32 |

^a The population of the C positions was equally distributed between the C1-Cu and C2-Cu sites.

^b The overall values were obtained assuming a uniform monolayer coverage on all sites considering the population of each site as its weight factor.

Also listed in Table 6 are the overall values of the energetic data which were obtained through averaging of the individual values of the available sites according to their population contributions in the zeolite matrix. The populations were found by counting the number of each site in a doubled unit cell. Table 6 also reports the Cu⁺ binding energy for the studied CuZ clusters. As evident, the binding energy ranged from 146.99 to 195.45 kcal/mol where the highest and the lowest values were assigned to the M3-Cu and M1-Cu sites, respectively. This strongest binding is followed by the A-Cu, C1-Cu and I-Cu sites, with the Cu-Z dissociation energies of 179.71, 174.79, and 174.01 kcal/mol, respectively, such that the overall sequence becomes M1 < C2 < M4 < M2 < I < C1 < A < M3. Indeed, the Cu⁺ ion is most strongly bound in the 6T rings of the zeolite network. As mentioned previously, the 6T ring of the ZSM-11 structure (M3) is also the most reactive position to the Cu cation and a relatively small reaction heat is required for an exchange at this location. These findings partially resemble the data reported previously by Nachtigalova et al. [31] for the Cu²⁺ ion which was observed to bind more strongly to the 6T-rings of an Al-containing MFI structure. Similar findings have been reported by Rejmak et al. [18] for the exchanged Cu⁺ ions in an

Al-incorporated faujasite. As far as we know, however, the relatively similar preference of the copper ion for the intersection sites of ZSM-11 is a new finding. The relatively strong bindings offered by the intersection sites to the impregnating copper ion finds more importance when taking into consideration that this site constitutes a large portion of the available positions of the zeolite structure (Table 6). The di-coordinated Cu⁺ ions at the intersection sites have a high accessibility and are expected to be involved in the catalytic activity of the copper-exchanged zeolite [28]. However, the overall behavior of the solid matrix as estimated from a population average of the energetic data lies between the values obtained for M3-Cu and I-Cu when the exchange enthalpies are compared and would be closest to the corresponding values of M2-Cu, I-Cu, and C1-Cu in terms of the binding energy. Therefore, the mentioned sites might be chosen as a representative of the whole material in possible required simplifications depending upon which energetic property has to be assessed.

All but one of the sites available in the ZSM-11 structure (M3) provide a weaker binding for Cu⁺ than the alpha site (A). However, both the Cu⁺/H⁺ exchange enthalpies of the A-Cu site (126.17 kcal/mol) and that of a typical ZSM-11 matrix (124.84 kcal/mol) are interestingly higher than the exchange energies of 43.0–102.2 kcal/mol calculated for Cu²⁺ ions exchanged to H-ZSM-5 [31] but closer to other values reported earlier such as a 96.3–124.6 kcal/mol for Cu⁺ in ZSM-5 by Blint [46]. The observed differences can be only partially attributed to the oxidation state of the copper in the work by Nachtigalova et al. [31] which replaces two protons with a strongly bound Cu²⁺ ion as a [Z-O]-Cu-[O-Z] complex and, therefore, reduces the exchange energy with respect to that of a Cu⁺ ion. The aliasing effect of the computational method employed is worth attention as well which calls for further theoretical research in this respect. However, the main source of difference might be the effect of framework type assuming that the effects of method and the cluster size are negligible.

The binding energies reported in Table 6 can also be compared against similar magnitudes from the literature including 482–715 kcal/mol for the optimized Cu²⁺ coordination in ZSM-5 [24], about 139 kcal/mol for Cu⁺ ions in ZSM-5 [28], 109.6–136.9 kcal/mol for Cu⁺ ions in ZSM-5 [110], 169.5 kcal/mol for Cu-Y [14], 106.1–146.7 kcal/mol for Cu⁺ binding in FER [29], and a 163.9 kcal/mol binding energy for Cu⁺ in ZSM-5 [15]. As can be seen, all of the previously reported data for the binding energy of Cu⁺ ion particularly the last report are very close to the range obtained here for the various sites of ZSM-11. The corresponding magnitudes reported by Groothaert et al. [24] for Cu²⁺ ions bound to the oxide surface of ZSM-11 with two Al atoms incorporated have been significantly larger than those of Cu⁺ ion. Rejmak et al. [18] have also found that the strength of cation binding should increase with the number of Al atoms present in the 6T rings of a faujasite. These

confirm our discussion just presented above to explain the source of differences in the energetic data.

Also worth noting is that the average of the energetic data for a Cu-ZSM-11 catalyst is slightly smaller than that of the alpha site from a Cu-ZSM-5 catalyst. It might be concluded with some caution that the chemical or geometrical nature of the available sites in ZSM-11 would only partially account for the experimentally observed higher sorption power and reactivity of the MEL structure in the decomposition of NO and N₂O molecules with respect to those of Al-containing MFI zeolites (if can be compared on a sound basis). Then, it appears up to now that the main factor which plays the role in this privilege is the better accessibility of the reactant/template molecules to the available sites. However, the superior activity of Cu-ZSM-11 relative to Cu-ZSM-5 in direct N₂O decomposition has been attributed to both a higher accessibility and a better reducibility of Cu⁺ species, implying that the framework topologies of the zeolites would influence the reducibility of Cu⁺ species present on the copper-ion-exchanged zeolites [55]. A more precise evaluation of the two catalysts requires, at least, a similar systematic study of the MFI zeolite to be implemented with the energy of binding or the exchange energy averaged over the available sites as it was conducted for MEL, however. Further works in the same line are then required to gain a more detailed and deeper insight into the mechanistic role of the active site for the design and development of selective catalysts.

Conclusion

This paper investigated the geometrical, electronic, and energetic properties of Cu⁺ monoatomic centers in Cu-ZSM-11 catalysts using the cluster modeling approach through density functional theory. Total of 7 sites for Cu⁺ exchange to H-ZSM-11 were considered and compared with an alpha-site from an MFI structure. The coordination numbers differed from two to four, with the former observed at the intersections, the 4T-rings, and the basket-like positions of ZSM-11 and the latter in the other ring sites and cage-like locations. The HOMO–LUMO energy gaps of the copper-exchanged clusters fell into the range of 3.31–5.15 eV at the TD-BH&HLYP/6-311+G* level. Overall, the I–Cu and M1–Cu clusters were the highest polarizable sites and M4–Cu was found to be the most stable site as indicated from the HOMO–LUMO gaps. In total, the QTAIM results manifested closed-shell electrostatic interactions for all of the sites. The charge transfer varied from 0.10 e to 0.33 e with the highest value belonging to the cage-like positions which provided weakly bounded tri- and tetra-coordinated planar configurations with the nearest-neighbor oxygen atoms of the surface. Excellent power-type correlations were observed between the electronic properties and the bond distances. The exchange enthalpy ranged from 108.93 to 141.14 kcal/mol. The 6T-ring was the most readily exchangeable site while the 4T-ring site was the least favorable thermodynamically. As far as the most accessible sites for a

coming molecule are concerned, both M3 and I positions are adequately readily exchanged, however. The binding energy was found to alter in the range of 146.99–195.45 kcal/mol. As revealed from the energetic data, the Cu⁺ ion most strongly bound in the 6T rings followed by the cages and the intersections of the zeolite matrix.

Computational method

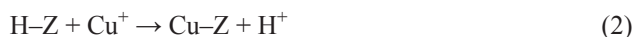
The cluster modeling method was employed for the molecular simulations. As a common approach to mimic the influence and rigidity of the surrounding framework [4, 15, 20, 24, 31, 33, 110–120], all of the dangling bonds at the boundaries of every cluster were terminated by link hydrogen atoms placed in the same bond direction as would be found in a perfect crystal for the next oxygen or silicon atom removed from the cluster. The boundary H atoms were placed at 0.960 and 1.550 Å from the oxygen and silicon atoms, respectively, with the values determined from preliminary optimizations. In total, the size of the clusters ranged from a T5 to a T10 unit. Here, every cluster model incorporates an aluminum atom that requires a compensating ion on one of the adjacent oxygen atoms. The crystallographic data for the frameworks of ZSM-11 and ZSM-5 can be found elsewhere [121–122]. In addition to the exchange positions introduced in Fig. 1, a separate fragment from an MFI structure was also modeled for comparison. This cluster was taken from an alpha position—an effective 6T-ring on the wall of straight channel, formed by two interconnecting 5T-rings, and readily available to reagents—which appears to be of special interest with respect to catalytic actions [17, 20, 24, 119–120, 123–125]. The exchanged/compensating ion was taken here to be a Cu⁺ or an H⁺ ion as the key element of the active site. These cluster models are adequate to explain the interactions of the metal ion with the oxide surface within a precise local picture of the active site [33, 126–127]. A two-step optimization procedure was used. At the first stage, all of the atoms in the cluster except the Cu ion, proton, and Al atom were fixed during the geometrical optimizations to simply represent the mechanical embedding of the solid matrix. At the second step, the nearest interacting oxygen atoms were also relaxed to include possible alterations in the skeletal vibrations due to the Al substitution or the Cu exchange.

The molecular geometries of the structures were optimized using the functional B3LYP method [86–87, 128] which has been reported to yield reliable data on both oxides and metal clusters [4, 23, 129]. The Pople's standard 6-31+G* basis set [130–133] was employed for all of the atoms. The single-point calculations were implemented with a larger basis set at B3LYP/6-311+G* [134] for improved energetic data. Calculations were also made with the M06/Def2–TZVP method. The atomic charges for the optimized structures were obtained through the natural bond orbital (NBO) calculations. The energetic calculations were performed on the zeolite surface (Z⁻) excluding the metal ion (Cu⁺) to allow for an estimation of the binding energy (ΔE_b) of Cu⁺ at

every site [24], which was defined as the energy of the following reaction with a negative sign [18, 29, 110]:



The Cu⁺/H⁺ exchange enthalpy (ΔH_{ex}) was defined as the enthalpy change of the reaction [31]:



where symbols Cu-Z and H-Z refer to the copper-exchanged cluster and the acidic surface of the zeolite, respectively.

The NBO population [135] and the QTAIM [98-99, 136-139] assessments were done at the B3LYP/6-311+G* level of theory. The calculations were implemented using NWChem 6.5 [140] and Multiwfn 3.3.8 [141]. The graphical outputs were drawn by the molecular visualization program Mercury 3.3 [142-145].

References

- Smeets, P. J., et al. *Inorganic Chemistry*. **2010**, *49*, 3573-3583.
- Delabie, A., et al. *European Journal of Inorganic Chemistry*. **2002**, *2002*, 515-530.
- Pidko, E. A.; Hensen, E. J. M.; van Santen, R. A. *Proceedings of the Royal Society A: Mathematical, Physical and Engineering Science*. **2012**, *468*, 2070-2086.
- Ferullo, R. M., et al. *Journal of Molecular Structure: THEOCHEM*. **2006**, *769*, 217-223.
- Woertink, J. S., et al. *Proc Natl Acad Sci USA*. **2009**, *106*, 18908-18913.
- Gao, Y.; Kispert, L. D. *Dalton Transactions*. **2014**, *43*, 6221-6228.
- Davidová, M., et al. *The Journal of Physical Chemistry B*. **2004**, *108*, 13674-13682.
- Solans-Monfort, X., PhD Dissertation, in: *Departament de Química*, Universitat Autònoma de Barcelona, Bellaterra, **2003**.
- Sengupta, D., et al. *Catal Lett*. **2001**, *74*, 193-199.
- Kim, S. J., et al. *Journal of Nanoscience and Nanotechnology*. **2010**, *10*, 147-157.
- Kustova, M. Y., et al. *Applied Catalysis B: Environmental*. **2006**, *67*, 60-67.
- Mitra, S., MSc Thesis, in: *Department of Chemical Engineering*, National Institute of Technology, Rourkela, **2014**.
- Sierraalta, A.; Añez, R.; Brussin, M.-R. *Journal of Catalysis*. **2002**, *205*, 107-114.
- Sung, C.-Y., et al. *The Journal of Physical Chemistry C*. **2011**, *116*, 3561-3575.
- Treesukol, P.; Limtrakul, J.; Truong, T. N. *The Journal of Physical Chemistry B*. **2001**, *105*, 2421-2428.
- Ahmed, A. H. *Journal of Applied Sciences Research*. **2007**, *3*, 1663-1670.
- Pidko, E.; Kazansky, V. *Physical Chemistry Chemical Physics*. **2005**, *7*, 1939-1944.
- Rejmak, P.; Sierka, M.; Sauer, J. *Physical Chemistry Chemical Physics*. **2007**, *9*, 5446-5456.
- Berthomieu, D., et al. *The Journal of Physical Chemistry B*. **2001**, *105*, 1149-1156.
- Broclawik, E., et al. *Catalysis Today*. **2002**, *75*, 353-357.
- Bulanek, R., et al. *Physical Chemistry Chemical Physics*. **2004**, *6*, 2003-2007.
- Davidová, M., et al. *The Journal of Physical Chemistry B*. **2003**, *107*, 2327-2332.
- Ferullo, R. M.; Castellani, N. J. *Journal of Molecular Catalysis A: Chemical*. **2004**, *221*, 155-162.
- Groothaert, M. H., et al. *Physical Chemistry Chemical Physics*. **2003**, *5*, 2135-2144.
- Hagelberg, F.; Xiao, C.; Lester, W. A. *Physical Review B*. **2003**, *67*, 035426-1-035426-9.
- Kamarudin, K. S. N., PhD Dissertation, Universiti Teknologi Malaysia, **2009**.
- Kustova, M. Y., et al. *Catalysis Communications*. **2006**, *7*, 705-708.
- Morpurgo, S.; Moretti, G.; Bossa, M. *Theor Chem Account*. **2012**, *131*, 1-12.
- Nachtigall, P.; Davidová, M.; Nachtigallová, D. *The Journal of Physical Chemistry B*. **2001**, *105*, 3510-3517.
- Nachtigall, P.; Nachtigallová, D.; Sauer, J. *The Journal of Physical Chemistry B*. **2000**, *104*, 1738-1745.
- Nachtigallová, D.; Nachtigall, P.; Sauer, J. *Physical Chemistry Chemical Physics*. **2001**, *3*, 1552-1559.
- Pierloot, K., et al. *Physical Chemistry Chemical Physics*. **2001**, *3*, 2174-2183.
- Pietrzyk, P. *The Journal of Physical Chemistry B*. **2005**, *109*, 10291-10303.
- Ramstad, A. L.; Mikkelsen, Ø. *Journal of Molecular Structure*. **2004**, *697*, 109-117.
- Rice, M. J.; Chakraborty, A. K.; Bell, A. T. *The Journal of Physical Chemistry B*. **2000**, *104*, 9987-9992.
- Rice, M. J.; Chakraborty, A. K.; Bell, A. T. *Journal of Catalysis*. **2000**, *194*, 278-285.
- Sierraalta, A.; Bermudez, A.; Rosa-Brussin, M. *Journal of Molecular Catalysis A: Chemical*. **2005**, *228*, 203-210.
- Šponer, J. E., et al. *The Journal of Physical Chemistry B*. **2001**, *105*, 8285-8290.
- Rodriguez-Santiago, L., et al. *Journal of the American Chemical Society*. **1998**, *120*, 1545-1551.
- Sengupta, D., et al. *Catal Lett*. **1999**, *61*, 179-186.
- Schneider, W. F., et al. *The Journal of Physical Chemistry B*. **1998**, *102*, 3692-3705.
- Tajima, N., et al. *Physical Chemistry Chemical Physics*. **1999**, *1*, 3823-3830.
- Hass, K. C.; Schneider, F. W. *Physical Chemistry Chemical Physics*. **1999**, *1*, 639-648.
- Schneider, W. F., et al. *The Journal of Physical Chemistry B*. **1997**, *101*, 4353-4357.
- Goodman, B. R., et al. *The Journal of Physical Chemistry B*. **1999**, *103*, 10452-10460.
- Blint, R. J. *The Journal of Physical Chemistry*. **1996**, *100*, 19518-19524.
- Yokomichi, Y., et al. *The Journal of Physical Chemistry*. **1996**, *100*, 14424-14429.
- Ramprasad, R., et al. *The Journal of Physical Chemistry B*. **1997**, *101*, 1940-1949.
- Schneider, W. F., et al. *The Journal of Physical Chemistry*. **1996**, *100*, 6032-6046.
- Hass, K. C.; Schneider, W. F. *The Journal of Physical Chemistry*. **1996**, *100*, 9292-9301.

51. Rice, M. J.; Chakraborty, A. K.; Bell, A. T. *The Journal of Physical Chemistry A*. **1998**, 102, 7498-7504.
52. Jacobs, P. A.; Martens, J. A. *Synthesis of High-Silica Aluminosilicate Zeolites*. Amsterdam: Elsevier, **1987**.
53. Fyfe, C. A., et al. *Journal of the American Chemical Society*. **1989**, 111, 2470-2474.
54. Čejka, J.; Corma, A.; Zones, S. *Zeolites and Catalysis: Synthesis, Reactions and Applications*. Weinheim: Wiley, **2010**.
55. Xie, P., et al. *Microporous and Mesoporous Materials*. **2014**, 191, 112-117.
56. Kustova, M. Y.; Hasselriis, P.; Christensen, C. H. *Catal Lett*. **2004**, 96, 205-211.
57. Ghashghaee, M.; Ghambarian, M.; Azizi, Z. *Struct Chem*. **2016**, 27, 467-475.
58. Sánchez, M., et al. *Microporous and Mesoporous Materials*. **2015**, 203, 91-99.
59. Gonzalez, G., et al. *Microporous and Mesoporous Materials*. **2009**, 121, 26-33.
60. Auerbach, S. M.; Carrado, K. A.; Dutta, P. K. *Handbook of Zeolite Science and Technology*. New York: Marcel Dekker, **2003**.
61. van der Gaag, F. J., **1987**.
62. Flanigen, E. M. *Pure & Appl. Chem*. **1980**, 52, 2191-2211.
63. Čejka, J.; Kubička, D., in: *Kirk-Othmer Encyclopedia of Chemical Technology*, John Wiley & Sons, Hoboken, New Jersey, **2010**, 1-30.
64. Xu, R., et al. *Chemistry of Zeolites and Related Porous Materials: Synthesis and Structure*. Singapore: John Wiley & Sons, **2007**.
65. Weitkamp, J.; Hunger, M. *Stud. Surf. Sci. Catal*. **2007**, 168, 787-835.
66. Guisnet, M.; Gilson, J.-P. *Zeolites for Cleaner Technologies*. London: Imperial College Press, **2002**.
67. Ghambarian, M., et al., in: *3rd International Congress of Chemistry and Chemical Engineering*, Tehran, Iran, **2016**, 292-299.
68. Ghashghaee, M., et al., in: *3rd International Congress of Chemistry and Chemical Engineering*, Tehran, Iran, **2016**, 188-195.
69. Sastre, G.; Corma, A. *Journal of Molecular Catalysis A: Chemical*. **2009**, 305, 3-7.
70. Derouane, E. G. *Chemical Physics Letters*. **1987**, 142, 200-204.
71. Boekfa, B., et al. *The Journal of Physical Chemistry C*. **2010**, 114, 15061-15067.
72. Derouane, E. G.; Chang, C. D. *Microporous and Mesoporous Materials*. **2000**, 35-36, 425-433.
73. Zicovich-Wilson, C. M.; Corma, A.; Viruela, P. *The Journal of Physical Chemistry*. **1994**, 98, 10863-10870.
74. Corma, A. *Journal of Catalysis*. **2003**, 216, 298-312.
75. Wongthong, P., Vol. MSc, Kasetsart University, **2005**.
76. Arifin, R., et al. *The Journal of Physical Chemistry C*. **2015**, 119, 3210-3216.
77. Eun Jee, S.; McGaughey, A. J. H.; Sholl, D. S. *Molecular Simulation*. **2009**, 35, 70-78.
78. García-Sánchez, A.; Dubbeldam, D.; Calero, S. *The Journal of Physical Chemistry C*. **2010**, 114, 15068-15074.
79. Krishna, R.; van Baten, J. M. *The Journal of Physical Chemistry C*. **2010**, 114, 18017-18021.
80. Handzlik, J.; Grybos, R.; Tielens, F. *The Journal of Physical Chemistry C*. **2013**, 117, 8138-8149.
81. Ghambarian, M.; Azizi, Z.; Ghashghaee, M. *Computational Materials Science*. **2016**, 118, 147-154.
82. Balar, M.; Azizi, Z.; Ghashghaee, M. *Journal of Nanostructure in Chemistry*. **2016**, 6, 365-372.
83. Göttl, F.; Hafner, J. *The Journal of Chemical Physics*. **2012**, 136, 064501-1-064501-17.
84. Göttl, F.; Hafner, J. *The Journal of Chemical Physics*. **2012**, 136, 064503.
85. Zhang, G.; Musgrave, C. B. *The Journal of Physical Chemistry A*. **2007**, 111, 1554-1561.
86. Lee, C.; Yang, W.; Parr, R. G. *Physical Review B*. **1988**, 37, 785-789.
87. Becke, A. D. *The Journal of Chemical Physics*. **1993**, 98, 5648-5652.
88. Gázquez, J. L.; Cedillo, A.; Vela, A. *The Journal of Physical Chemistry A*. **2007**, 111, 1966-1970.
89. Orozco-Valencia, Á. U.; Vela, A. *Journal of the Mexican Chemical Society*. **2012**, 56, 294-301.
90. Li, K.; Li, M.; Xue, D. *Nanoscale Research Letters*. **2012**, 7, 6.
91. Morell, C., et al. *Physical Chemistry Chemical Physics*. **2014**, 16, 26832-26842.
92. Fukui, K.; Yonezawa, T.; Shingu, H. *The Journal of Chemical Physics*. **1952**, 20, 722-725.
93. Pearson, R. G. *Journal of Chemical Education*. **1987**, 64, 561-567.
94. Parr, R. G.; Weitao, Y. *Density-Functional Theory of Atoms and Molecules*. New York: Oxford University Press, **1989**.
95. Vektariene, A.; Vektaris, G.; Svoboda, J. *ARKIVOC*. **2009**, 7, 311-329.
96. Gopalakrishnan, S. B.; Kalaiarasi, T.; Subramanian, R. *Journal of Computational Methods in Physics*. **2014**, 2014, 623235-1-623235-6.
97. Aihara, J.-i. *The Journal of Physical Chemistry A*. **1999**, 103, 7487-7495.
98. Bader, R. F. W. *Atoms in Molecules: A Quantum Theory*. USA: Oxford University Press, **1994**.
99. Matta, C. F.; Boyd, R. J. *The Quantum Theory of Atoms in Molecules: From Solid State to DNA and Drug Design*. Weinheim: Wiley-VCH Verlag GmbH & Co. KGaA, **2007**.
100. Lopez, N., et al. *Chemical Physics Letters*. **1998**, 294, 611-618.
101. Lopez, N.; Illas, F.; Pacchioni, G. *The Journal of Physical Chemistry B*. **1999**, 103, 1712-1718.
102. Padilla-Campos, L. *Journal of the Chilean Chemical Society*. **2005**, 50, 745-752.
103. Burda, J. V.; Shukla, M. K.; Leszczynski, J. *J Mol Model*. **2005**, 11, 362-369.
104. Halbert, S.; Gerard, H. *New Journal of Chemistry*. **2015**, 39, 5410-5419.
105. Gibbs, G. V., et al. *The Journal of Physical Chemistry B*. **2003**, 107, 12996-13006.
106. Gibbs, G. V., et al. *zkri*. **2008**, 223, 1-40.
107. Gálvez, O.; Gómez, P. C.; Pacios, L. F. *The Journal of Physical Chemistry*. **2003**, 118, 4878-4895.
108. Lü, R., et al. *Bulletin of the Korean Chemical Society*. **2013**, 34, 1814-1822.
109. Gibbs, G. V., et al. *The Journal of Physical Chemistry B*. **2005**, 109, 21788-21795.
110. Nachtigallova, D., et al. *Physical Chemistry Chemical Physics*. **1999**, 1, 2019-2026.
111. Aleksandrov, H. A.; Vayssilov, G. N.; Rösch, N. *Journal of Molecular Catalysis A: Chemical*. **2006**, 256, 149-155.
112. Pidko, E. A.; van Santen, R. A. *The Journal of Physical Chemistry C*. **2007**, 111, 2643-2655.
113. Yakovlev, A., et al. *Catal Lett*. **2000**, 70, 175-181.
114. Yang, G., et al. *Journal of Molecular Catalysis A: Chemical*. **2005**, 237, 36-44.
115. Dědeček, J., et al. *The Journal of Physical Chemistry C*. **2009**, 113, 1447-1458.
116. Lesthaeghe, D., et al. *ChemCatChem*. **2011**, 3, 208-212.

117. Wesolowski, T. A.; Goursoot, A.; Weber, J. *Journal of Chemical Physics*. **2001**, *115*, 4791-4797.
118. Zhang, B., et al. *Journal of Environmental Sciences*. **2011**, *23*, 681-686.
119. Zhidomirov, G. M., et al. *International Journal of Quantum Chemistry*. **2004**, *100*, 489-494.
120. Shubin, A. A., et al. *Catal Lett*. **2003**, *90*, 137-142.
121. Terasaki, O., et al. *Chemistry of Materials*. **1996**, *8*, 463-468.
122. van Koningsveld, H.; Jansen, J. C.; van Bekkum, H. *Zeolites*. **1990**, *10*, 235-242.
123. Zhidomirov, G. M.; Shubin, A. A.; van Santen, R. A., in: *Computer Modelling of Microporous Materials*, Catlow, C. R. A., van Santen, R. A., and Smit, B. Eds., WILEY-VCH Verlag, **2005**, 201-241.
124. Heyden, A., PhD Dissertation, in: *Department of Chemical Reaction Engineering*, Hamburg University of Technology, Hamburg, **2005**.
125. Mikhailov, M. N., et al. *Microporous and Mesoporous Materials*. **2007**, *104*, 145-150.
126. Pietrzyk, P., et al. *The Journal of Physical Chemistry B*. **2003**, *107*, 6105-6113.
127. Chester, A. W.; Derouane, E. G. *Zeolite Characterization and Catalysis: A Tutorial*. Dordrecht: Springer, **2009**.
128. Becke, A. D. *Physical Review A*. **1988**, *38*, 3098-3100.
129. Yumura, T., et al. *Physical Chemistry Chemical Physics*. **2010**, *12*, 2392-2400.
130. Hariharan, P. C.; Pople, J. A. *Molecular Physics*. **1974**, *27*, 209-214.
131. Francl, M. M., et al. *The Journal of Chemical Physics*. **1982**, *77*, 3654-3665.
132. Clark, T., et al. *Journal of Computational Chemistry*. **1983**, *4*, 294-301.
133. Frisch, M. J.; Pople, J. A.; Binkley, J. S. *The Journal of Chemical Physics*. **1984**, *80*, 3265-3269.
134. Kendall, R. A.; Dunning, T. H.; Harrison, R. J. *The Journal of Chemical Physics*. **1992**, *96*, 6796-6806.
135. Glendening, E., et al. *Theoretical Chemistry Institute, University of Wisconsin, Madison, WI*. **1996**.
136. Rodríguez, J. I., et al. *Chemical Physics Letters*. **2009**, *472*, 149-152.
137. Bader, R. F. W. *Chemical Reviews*. **1991**, *91*, 893-928.
138. Bader, R. F. W. *Monatshefte für Chemie*. **2005**, *136*, 819-854.
139. Bader, R. F. W. *Accounts of Chemical Research*. **1975**, *8*, 34-40.
140. Valiev, M., et al. *Computer Physics Communications*. **2010**, *181*, 1477-1489.
141. Lu, T.; Chen, F. *Journal of Computational Chemistry*. **2012**, *33*, 580-592.
142. Bruno, I. J., et al. *Acta Crystallographica Section B*. **2002**, *58*, 389-397.
143. Macrae, C. F., et al. *Journal of Applied Crystallography*. **2008**, *41*, 466-470.
144. Macrae, C. F., et al. *Journal of Applied Crystallography*. **2006**, *39*, 453-457.
145. Taylor, R.; Macrae, C. F. *Acta Crystallographica Section B*. **2001**, *57*, 815-827.